Journal of Power Sources 196 (2011) 4209–4217

Contents lists available at ScienceDirect

Journal of Power Sources

journal homepage: www.elsevier.com/locate/jpowsour

Study of flow channel geometry using current distribution measurement in a high temperature polymer electrolyte membrane fuel cell

Justo Lobato*, Pablo Cañizares, Manuel A. Rodrigo, F. Javier Pinar, Diego Úbeda

Chemical Engineering Department, University of Castilla-La Mancha, Enrique Costa Novella Building, Avda. Camilo José Cela, n 12, 13071, Ciudad Real, Spain

ARTICLE INFO

Article history:
Received 29 July 2010
Received in revised form 9 September 2010
Accepted 4 October 2010
Available online 13 October 2010

Keywords:
Channel geometry
PBI
Current distribution
High temperature PEMFC

ABSTRACT

To improve fuel cell design and performance, research studies supported by a wide variety of physical and electrochemical methods have to be carried out. Among the different techniques, current distribution measurement owns the desired feature that can be performed during operation, revealing information about internal phenomena when the fuel cell is working. Moreover, short durability is one of the main problems that is hindering fuel cell wide implementation and it is known to be related to current density heterogeneities over the electrode surface. A good flow channel geometry design can favor a uniform current density profile, hence hypothetically extending fuel cell life. With this, it was thought that a study on the influence of flow channel geometry on the performance of a high temperature polymer electrolyte membrane (PEM) fuel cell using current distribution measurement should be a very solid work to optimize flow field design. Results demonstrate that the 4 step serpentine and pin-type geometries distribute the reactants more effectively, obtaining a relatively flat current density map at higher current densities than parallel or interdigitated ones and yielding maximum powers up to 25% higher when using oxygen as comburent. If air is the oxidant chosen, interdigitated flow channels perform almost as well as serpentine or pin-type due to that the flow conditions are very important for this geometry.

1. Introduction

It has been widely demonstrated that fuel cells are suitable to be used in several technological fields that cover from stationary to mobile applications. Around the world there are some power stations and residential zones that incorporate fuel cells to obtain electricity and even fuel cell-driven public transport or prototype vehicles can be found [1–4]. However, some steps remain in order to reach a high degree of commercialization, as problems related to operation and costs have to be overcome for fuel cells to be presented as a real substitute of turbines, combustion engines or conventional batteries. To achieve a comprehensive understanding of the processes occurring inside a fuel cell is crucial to detect the origin of some problems which solution would mean a true improvement in the device performance. To that end, researchers use an extended range of electrochemical, physical and chemical methods [5,6].

Regarding polymer electrolyte membrane (PEM) fuel cells and more specifically high temperature PEM fuel cells, one of their main problems lies on their durability. Besides other known reasons, the membrane–electrode-assembly (MEA) degradation is strongly linked to the existence of current heterogeneities in the electrode surface. This is mainly due to that properties and variables are not the same over the whole fuel cell area and therefore electrochemical reactions do not take place to the same extent in every point. Many of the actual analysis methods can be used to study the fuel cell performance at surface scale, however, some of them imply that operation has to be stopped or subject to the measurement process itself. On the contrary, current distribution mapping can be used during fuel cell operation and supply with information about internal phenomena. To measure current distribution there are various methods that have been developed under the years and which different characteristics should be considered in order to find a balance between advantages and drawbacks of each one. Excepting magnetotomography [7], no other non-invasive method has been found in scientific literature so it can be said that the vast majority of techniques require to set up the fuel cell specially for the measurement. These invasive methods could also be classified according to the degree of modification of the fuel cell respecting the one that would operate without a measurement system coupled. There are techniques that demand segmenting either the electrodes or the whole MEA and even the flow field plates in order to measure local current [8,9]. By doing this, current distribution map obtained should be very similar to the one that is actually been generated over the catalyst surface, as lateral currents are minimized. On the other hand, the fuel cell is completely modified and hence it is prob-

* Corresponding author. Tel.: +34 926 29 53 00x6707; fax: +34 926 29 52 56.
E-mail address: Justo.Lobato@uclm.es (J. Lobato).

0378-7753/$ – see front matter © 2010 Elsevier B.V. All rights reserved.
doi:10.1016/j.jpowsour.2010.10.017

able that the current profile differs from the one produced when segmentation does not exist. Other methods propose to segment only the current collector [10,11], or to use a printed circuit board located behind the flow field plate in a way that current distribution is only measured when it has crossed that one [12]. Like this, the fuel cell core remains unchanged but the current distribution map is not exactly the same as in the catalyst surface, since the measurement plane is relatively far and electron deviations may have occurred in their way from the catalyst to the current collector. Recently, Liu et al. [13] have tested a new method consisting of a current distribution measurement gasket which is inserted between the gas diffusion layer (GDL) and the flow field plate, evaluating then the local current very close to where it is actually produced without sectioning any of the fuel cell components.

In the present work, the influence of the flow channel geometry on the performance of a high temperature PBI-based PEM fuel cell has been studied using current distribution measurement. As it has been mentioned above, the degradation of these devices is accelerated when an uneven current density is being generated. A good flow channel configuration may help to achieve a flatter current distribution map during operation due to a good distribution of reactants over the electrode surface. Furthermore, higher power density can be obtained if an adequate flow field design is used in a fuel cell [14].

There are some works about flow channel geometry optimization for conventional PEM fuel cells [15,16]. Nevertheless, the well-known differences between operating at temperature lower or higher than water boiling point suggest that it is not reasonable to extrapolate those results to high temperature PEM fuel cells.

2. Experimental issues

2.1. Current distribution measurement technique

The method chosen to measure current distribution was a 49 cm^2 sensor plate formed by an array of 100 sensors equally distributed. This is a standard method developed by the company S++ which measurement principle is based upon the dependency of the permeability of a magnetically soft material on the magnetization and temperature. Each sensor consists basically of coils on a core made of magnetically soft material. Fig. 1 shows a photograph of the sensor plate and a scheme of its placement inside the fuel cell. The sensors individually measure the total current that is flowing through the plate portion where they are located. Thus, current distribution maps are obtained by graphically representing each total current data and the position of the sensor that measured it. The sensor plate is placed behind the flow field plate of the cathode side, so in this case it detects the electrons coming from the external circuit and leading to the cathode catalyst layer. A data acquisition board is connected to the sensor plate and current distribution maps are saved in a CPU using special software. Measurements may be single or continuous with a temporal resolution of 0.5 s.

The motivation for choosing this kind of technique comes from the intention of sticking to the following requisites reported on different scientific works that a current distribution method and the measured object should meet [17,18]:

(i) The MEA is the object of measurement and therefore it should not be modified. Segmenting the MEA would cause current distribution at the current collector to be different from the one produced in an unmodified fuel cell.
(ii) Flow field plates should keep their thermal and electric conductivities, as well as their gas distribution properties.
(iii) High spatial resolution in order to detect pronounced gradients.
(iv) High temporal resolution to make dynamic measurements.
(v) Measurement must not be influenced by operation.

With these precepts, segmenting MEA or flow field plates was discarded, whereas the other methods commented in Section 1 are in an early development stage or were not easily available. Thus, a similar method in terms of implementation to the used in [19] was selected. Apart from the previous guidelines, it is interesting that the method is easy to implement and data acquisition is very simple. As a drawback it has to be mentioned that the existence of lateral currents that affect the accuracy of the measurement has to be assumed. It leads to a loss in spatial resolution due to current spreading [20].

2.2. Preparation of membrane–electrode assemblies

The MEAs were totally self-manufactured and its fabrication process comprises preparing electrodes and membrane separately for its eventual union by means of hot-pressure.

In order to prepare the electrodes, the following procedure was followed. On top of a gas diffusion media (Toray Graphite Paper, TGPH-90, 250 h μm thick, 10% wet-proofing, ETEK, Inc.), a microporous layer (MPL) was deposited by N_2-spraying an ink consisting of 2 mg cm^{-2} Vulcan XC-72R Carbon Black (Cabot Corp.) and 10% PTFE (Teflon™ Emulsion Solution, Electrochem Inc.). Next, a catalyst layer, composed of Pt/C catalyst (40% Pt on Vulcan XC-72R Carbon Black, ETEK-Inc.) [21], PBI ionomer (1.24 wt.% PBI in *N,N′*-dimethylacetamide, DMAc), and DMAc as a dispersing solvent was also deposited by N_2-spraying. In all cases, the Pt loading on both electrodes was 0.25 mg Pt cm^{-2}, a C/PBI weight ratio of 20 was used [22], electrode area was 7×7 cm^2, the DMAc volume added as ink solvent was 25 ml and the platinum load was controlled by the electrode weight increase. After the deposition of the catalyst layer, the electrodes were dried at 190 °C for 2 h. Later, the electrodes were wetted with a solution of 1% H_3PO_4. Electrodes were left to absorb the acid one day.

For the preparation of the MEA, a PBI membrane which had been casted from a PBI solution synthesized from its monomers [23,24] was taken out from a 75 wt.% phosphoric acid bath. Doping level acquired by the membrane was 6.6 molecules of acid per polymer repeating unit. The superficial acid onto the membrane was thoroughly wiped off with filter paper, and subsequently, it was used to prepare the MEA. In order to fabricate it, the doped membrane was sandwiched between two electrodes, hot-pressing the whole system at 130 °C and 100 kg cm^{-2} for 15 min. Once the MEA was ready, it was inserted into the cell. The geometric area of the electrodes was 49 cm^2.

2.3. Experimental procedure

A MEA was inserted between two graphite end plates with the flow channels mechanized forming the desired geometry. Then, the sensor plate was placed behind the cathode sensor plate and a current collector was added to both parts of the fuel cell. Finally, two supporting plates with heaters and gas connections incorporated that provide also with mechanical support were mounted and screwed on with 8 bolts. Once the fuel cell is fully set up, a data acquisition board is connected to the sensor plate. All these articles were supplied by the company S++.

In order to perform the fuel cell tests, a potentiostat/galvanostat Autolab PGSTAT30 (Ecochemie, The Netherlands) with a Booster connected that allows to reach currents up to 20 A was used. Gas flows were regulated by two mass flow controllers from Brooks Instruments calibrated in the adequate flow ranges. Gas outlets were set to atmospheric pressure.

The tests itself started when the fuel cell had reached the working temperature (398 K in all the experiments), and gas flows were steady. At that moment, polarization curves were carried out until reproducibility was achieved. Current–potential pair values were

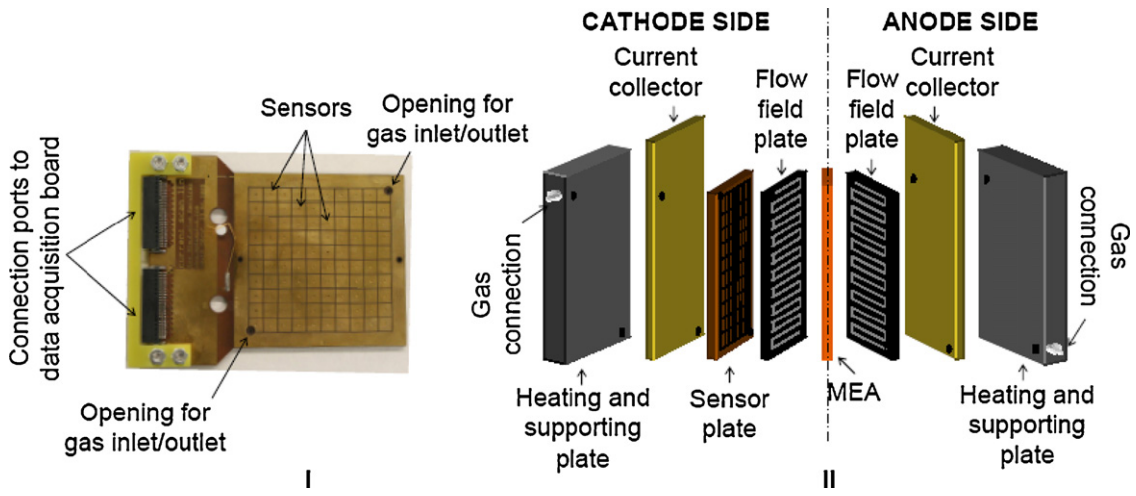

Fig. 1. (I) Photograph of the sensor plate and (II) descriptive sketch of its location and the rest of components of the single fuel cell.

recorded continuously, as well as current distribution maps. When a series of experiments with the same flow channel geometry were complete, the fuel cell was dismantled in order to substitute the final plate by other with a different geometry. During this process, the MEA was kept in exactly the same position so that possible heterogeneities that may exist due to its manual fabrication process would not mask the effects of flow channel configuration on the current distribution maps. When the fuel cell was set up again, it was made following exactly the same procedure as the explained in the first paragraph of this section and tightening with the same torque so that contact resistance was very similar in every case. Four different flow channel geometries were used, their scheme can be observed in Fig. 2 and geometric properties are given in Table 1.

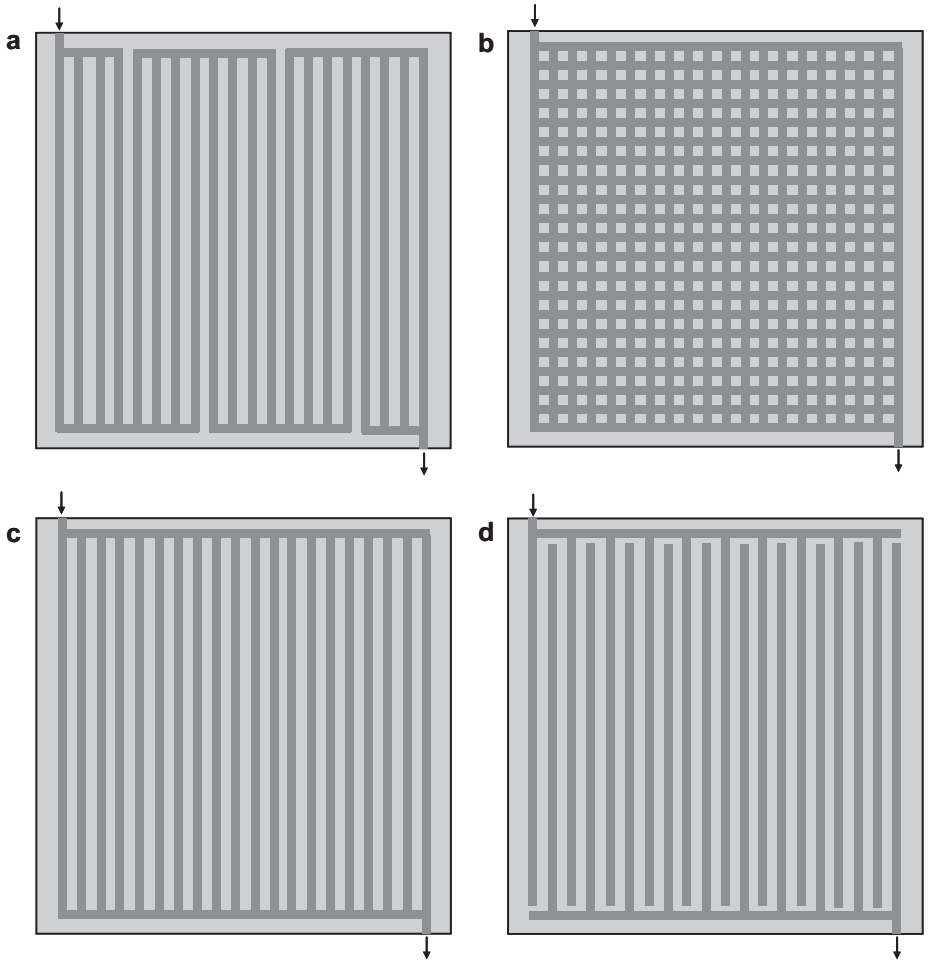

Fig. 2. Scheme of the four different flow channel geometries. (a) 4 step serpentine; (b) pin-type; (c) parallel and (d) interdigitated. Gas inlet and outlet are marked with arrows.

Table 1
Geometric properties of the flow field plates used.

Dimension	Value	Units
Channel width	1.5×10^{-3}	m
Land width	2×10^{-3}	m
Channel depth	1×10^{-3}	m
Flow field plate thickness	2×10^{-3}	m

Two different MEAs were used, one for the experiments with pure oxygen as oxidant and another for the experiments using air. MEAs were subject to a conditioning stage before using them for the first time. It consisted in keeping the fuel cell at 0.6 V during 24 h. This way later operation is more stable and reproducible, as during the first conditioning hours the MEA enhances its performance noticeably, reaching afterwards an almost steady state.

3. Results

3.1. Using pure oxygen as comburent

The main roles of flow channels in a fuel cell are to supply the system with reactants and to remove products from it, apart from ensure good electric and thermal conductivity. Therefore, it is evident that the differences between a good and a bad flow channel design will be more clearly appreciated when the fuel cell is working under conditions in which mass transport limitations are important. As the equipment used for this work could only reach 20 A, it was decided to limit the maximum total current to this value by introducing low reactant flow rates. This way, it is possible to perform polarization curves up to very low potential values and enabling then their comparison in all the regions. This flow limitation, together with the lower catalyst load, makes that the yields presented in this work are clearly poorer than those shown in [22] or [25].

Fig. 3 shows the polarization and power curves obtained for the four flow channel geometries used when the system is fed with an oxygen flow of 76 sccm. According to Faraday's law, the limit current for this flow rate is 20 A. Hydrogen in the anode side was introduced in excess.

As the same MEA was used in the four cases, the following statements can be formulated. For a given current value, activation overpotential must be very similar in all cases, since it depends only on catalyst aspects and MEAs were not used for such a long time that catalyst deactivation could be observed. Ohmic losses must also be the same in any case if the same current is flowing through the system, as flow field plates are made of the same material and therefore differences in conductivity should be negligible. Then, the deviations that can be seen for the polarization curves obtained using parallel and interdigitated flow channels regarding the ones for serpentine and pin-type are produced by a different concentration overpotential caused by the employ of a specific geometry. Serpentine and pin-type flow channels lead to an almost 25% higher maximum power than parallel or interdigitated flow channels. The reasons for these divergences can be more deeply analyzed by examining current distribution maps at different average current density levels.

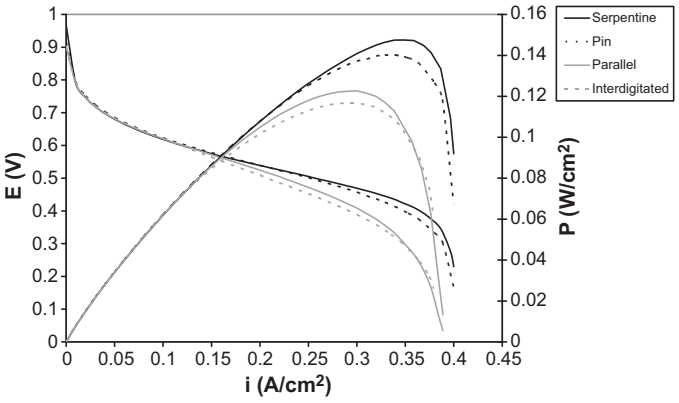

Fig. 3. Polarization and power curves obtained with different flow channel geometries. Oxygen flow rate was 76 sccm and hydrogen flow rate was 228 sccm.

Fig. 4 is an example of how current distribution maps will be presented. It has been elaborated with the intention of clarifying as much as possible the location of oxygen inlet and outlet and the way flow channels are positioned over the electrode, since these matters are important for the further interpretation of the current distribution maps. In Fig. 5, current distribution maps at an average current density of 0.1 A cm^{-2} are shown.

Although some heterogeneities in current density can be observed, maps in Fig. 5 are quite uniform. This can be explained because oxygen demand at this current level is low if compared to the oxygen flow entering the system and hence oxygen concentration variation from the inlet to the outlet is not important. Therefore it seems to be not important the way reactants are spread at low average current densities since any of the geometries tested causes an additional concentration overpotential. If the average current density is increased to 0.25 A cm^{-2}, the current distribution maps shown in Fig. 6 are obtained. In this case, current density profiles for serpentine and pin-type geometries are still very uniform, whereas the ones for parallel and interdigitated flow channels present patent gradients.

The low current density regions that can be appreciated are caused by a low oxygen concentration reaching the active catalyst sites over these areas and bring on higher concentration overpotentials and hence smaller fuel cell power, as can be observed in Fig. 3. Regarding parallel flow channels, the existence of paths through which gases flow preferentially is responsible for the development of a central zone where oxygen is more depleted, as already predicted by numerical simulations performed by this same research group [25]. Reactants flow at higher rate through peripheral channels, while smaller amounts circulate through central ones. Therefore, oxygen depletes very quickly in channels with low oxygen rates and then vapor water concentration grows fast, causing both a lower oxygen concentration at catalyst active sites and more difficult oxygen diffusion due to water presence. This uneven distribution induces an inefficient use of electrode area. When using interdigitated flow channels, the desired improvement in fuel cell performance by forcing gas convection through the GDL is not achieved, as phenomena of the same nature as preferential paths is probably occurring.

At 0.38 A cm^{-2}, the maximum average current density that could be measured for interdigitated flow channels, current distribution maps show more clear gradients for any geometry, as it can be seen in Fig. 7.

All current density profiles are influenced by oxygen depletion and consequent water formation and the shape they take agree totally with the way gases flow through the flow channels. Even so, variations are less pronounced in the case of serpentine and pin-type and therefore concentration overpotentials are lower still at this current level, which is very close to the limit.

With the intention of discarding that the differences observed between the four geometries were caused by MEA degradation, the first experiment was repeated after finishing all the ones previously commented. Results were almost identical, so the changes observed could be attributed to the different flow distribution and not to an improvement or worsening on MEA performance.

After the effects of a limiting oxygen flow rate were observed, the total fuel current was again limited to 20 A, this time by restrict-

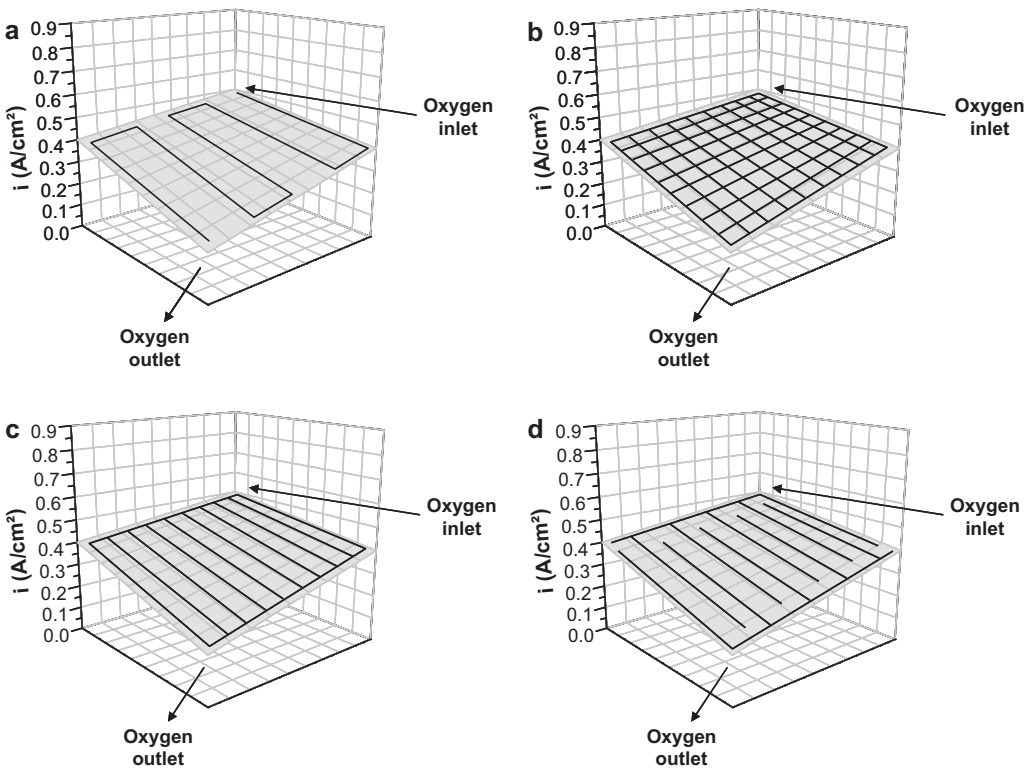

Fig. 4. Example figure of how current distribution maps are presented and outline of flow channel placement over the electrode and situation of oxygen inlet and outlet. (a) Serpentine; (b) pin-type; (c) parallel; and (d) interdigitated.

ing hydrogen flow rate to 152 sccm. Oxygen flow was doubled from the previous experiments. Fig. 8 shows the polarization and power curves obtained under these new conditions.

Looking at power peaks, it can be concluded that serpentine and pin-type flow channels give better results also under the new flow conditions. Nevertheless, in contrast to Fig. 3, the four polarization are almost the same up to high current density values. This can be explained because as hydrogen is a smaller molecule than oxygen, it diffuses more easily and hence mass transfer problems caused by the lack of this reactant will not appear unless the system is

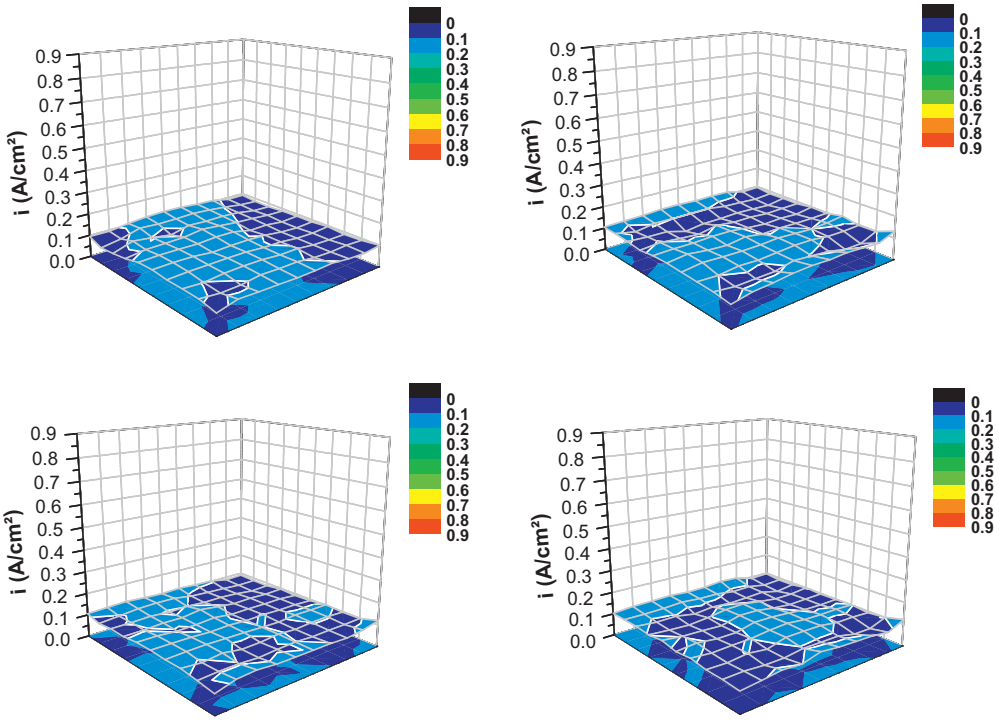

Fig. 5. Current distribution maps at an average current density of 0.1 A cm^{-2} under the flow conditions specified in Fig. 3. To find the correspondence between geometries and maps, refer to Fig. 4.

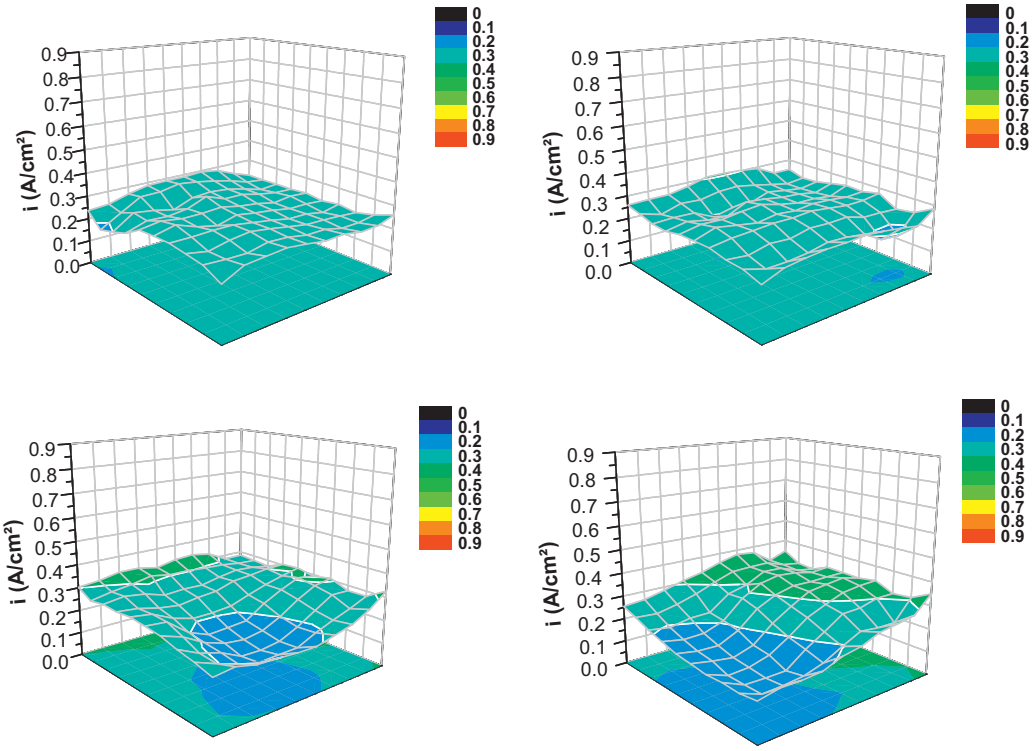

Fig. 6. Current distribution maps at an average current density of 0.25 A cm^{-2} under the flow conditions specified in Fig. 3. To find the correspondence between geometries and maps, refer to Fig. 4.

demanding a very high amount or it is completely depleted. In Fig. 9, current distribution maps at an average current density very close to the limit are presented. In this case, graphs have been rotated in order to orient hydrogen outlet to the front plane and get a better view.

The most important gradients can be noticed when parallel or interdigitated flow channels are used. Low current densities are measured near hydrogen outlet, which is due to its almost total depletion. However, if staring at interdigitated flow configuration map, a depressed region coincident with oxygen outlet can also

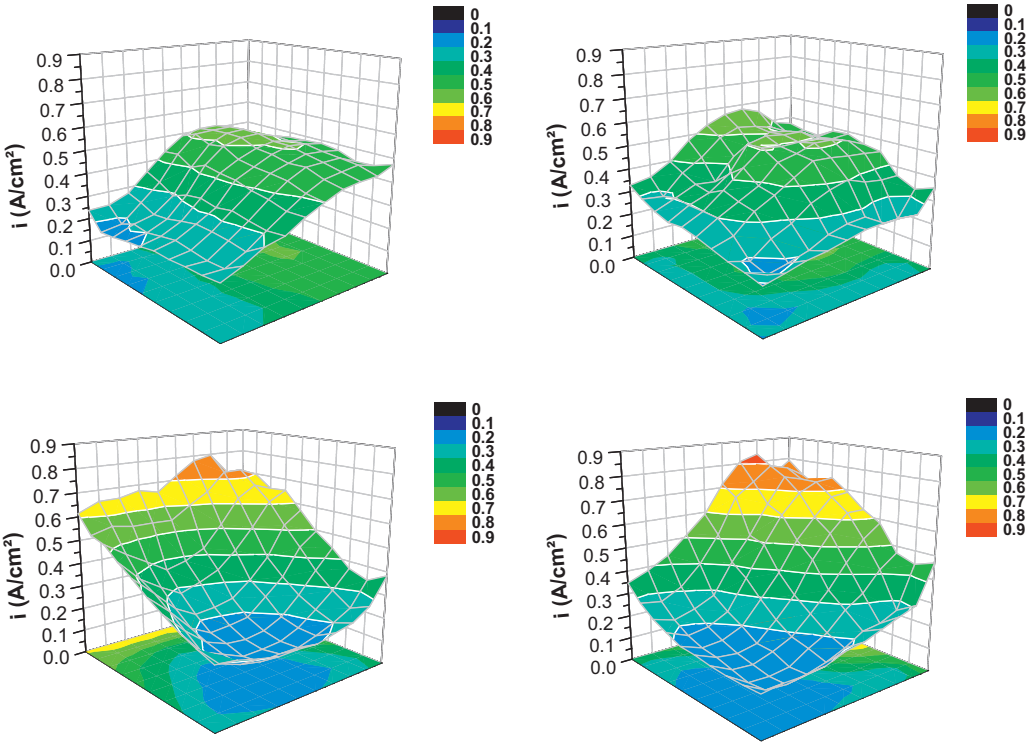

Fig. 7. Current distribution maps at an average current density of 0.38 A cm^{-2} under the flow conditions specified in Fig. 3. To find the correspondence between geometries and maps, refer to Fig. 4.

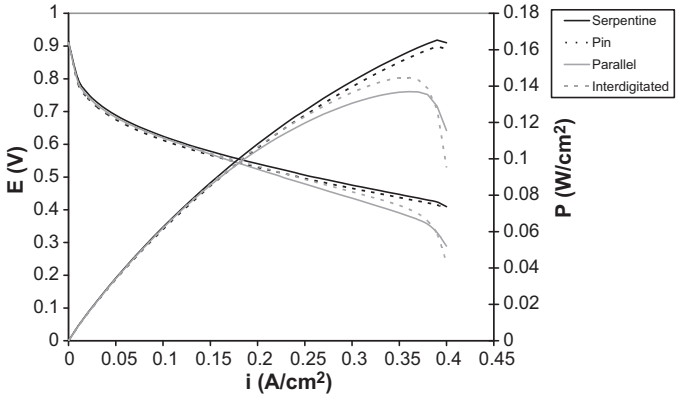

Fig. 8. Polarization and power curves obtained with different flow channel geometries. Both oxygen and hydrogen flow rates were 152 sccm.

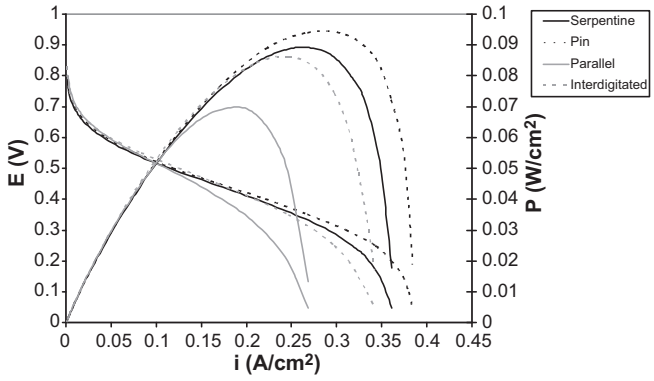

Fig. 10. Polarization and power curves obtained with different flow channel geometries. Air flow rate was 362 sccm and hydrogen flow rate was 228 sccm.

be observed. It means that in this case mass transfer overpotential is not only caused by lack of hydrogen, but also oxygen diffusion problems contribute to an efficiency loss although flow rate was multiplied by two. This is not so easy to see in the parallel flow channels map, as the low current density area due to oxygen depletion merges with the corresponding to hydrogen deficiency. For serpentine and pin-type flow channels it can be said that the efficient flow distribution achieved along with the very good diffusion of hydrogen make that mass transfer limitations are almost inexistent even at this high current density level.

3.2. Using air as comburent

In order to study the effects of oxygen dilution and a remarkable increment in gas flow rate, an air stream instead of pure oxygen was used to feed the cathode side. As oxygen concentration in air is approximately 20%, it has to bear in mind that in order to get the same amount of reactant, flow rate must be five times as much as if pure oxygen was employed, meaning then that flow conditions will change significantly in terms of Reynolds number. In the first experiment, current was limited to 20 A by restricting oxygen flow in air in the same way as in the previous cases. Results obtained when performing polarization curves are shown in Fig. 10.

First of all, it can be realized that the theoretical limit current is not achieved whatever the geometry used is. Dilution makes impossible to consume all the reactant. Here, pin-type flow channels behave slightly better than serpentine ones, but the fact that deserves more attention is that the fuel cell performs notably better with an interdigitated configuration than when parallel flow channels are set. This can be an indication of the beneficial consequences that increasing flow rate has on gas distribution when

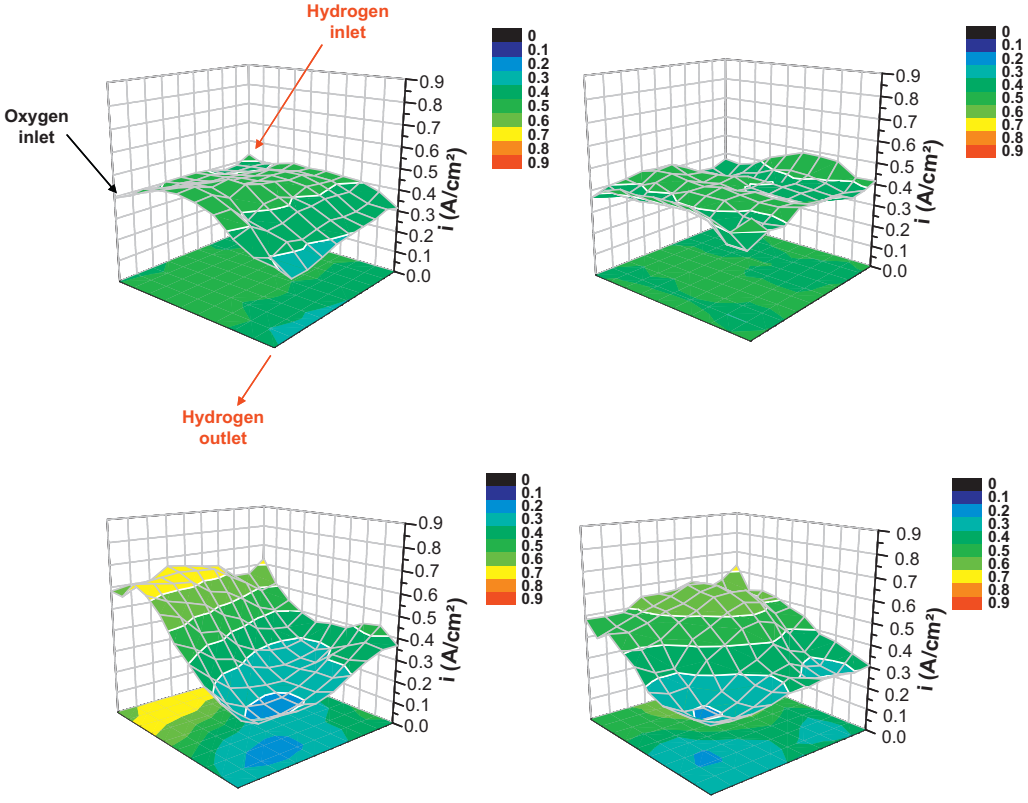

Fig. 9. Current distribution maps at an average current density of 0.39 A cm^{-2} under the flow conditions specified in Fig. 8. To find the correspondence between geometries and maps, refer to Fig. 4.

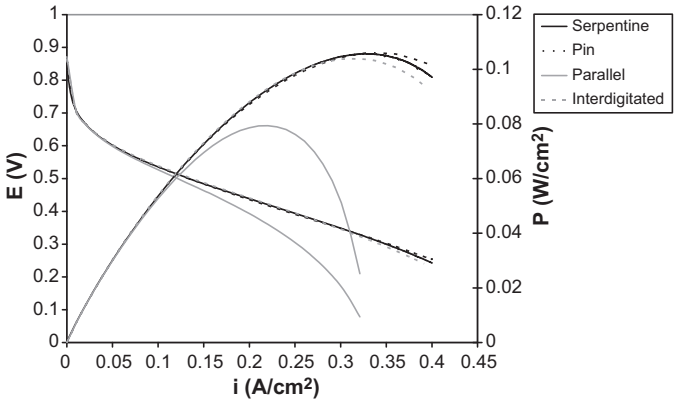

Fig. 11. Polarization and power curves obtained with different flow channel geometries. Air flow rate was 724 sccm and hydrogen flow rate was 228 sccm.

using interdigitated flow channels. Since inlet and outlet are not directly linked, gas is forced to pass through the GDL in order to abandon the system. With this, it is intended to favor convective flux to the catalyst layer, but while this effect is almost negligible at low flow rates, it can be clearly appreciated when flow conditions are completely altered. This assertion is confirmed if the flow rate is doubled respecting the used in Fig. 10, as it can be seen in Fig. 11, where very similar yields are measured for serpentine, pin-type and interdigitated flow channels. On the other hand, parallel flow channels keep on giving remarkably worse results, which suggests that this configuration is not influenced by flow settings.

In Fig. 12, current distribution maps at the maximum average current density obtained for parallel flow channels in Fig. 11 are presented.

While significantly big regions indicating mass transfer problems do no exist in serpentine, pin-type and interdigitated geometries as could be expected if looking at polarization curves, the map for parallel flow channels shows the same trend as the map displayed in Fig. 7. The main difference with the last one is that current density gradients are less steep although both maps are measured under high demand conditions. This is because concentration cannot vary in such a big range.

Table 2
Geometric properties of the different serpentine flow channels.

Name	Channel width	Channel depth	Units
A	1.5×10^{-3}	1×10^{-3}	m
B	1.5×10^{-3}	1.5×10^{-3}	m
C	2×10^{-3}	1×10^{-3}	m
D	2×10^{-3}	1.5×10^{-3}	m

Employing the same flow conditions as in the last experiment commented, a study of the influence of flow channel dimensions on the fuel cell performance was also carried out. The geometry chosen was the 4 step serpentine and the different channel dimensions tested can be checked in Table 2. Fig. 13 shows the results obtained.

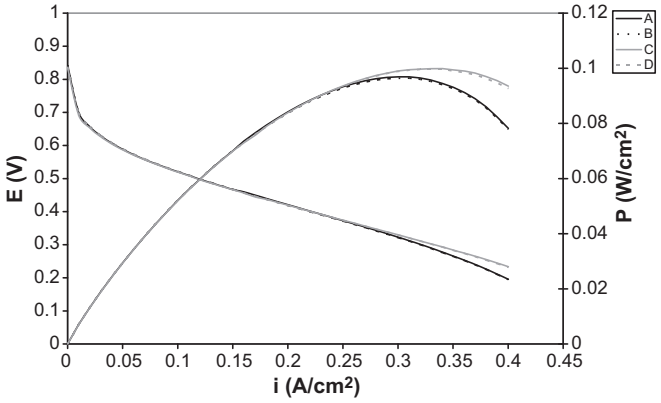

Fig. 13. Polarization and power curves obtained with different serpentine flow channel dimensions. Air flow rate was 724 sccm and hydrogen flow rate was 228 sccm.

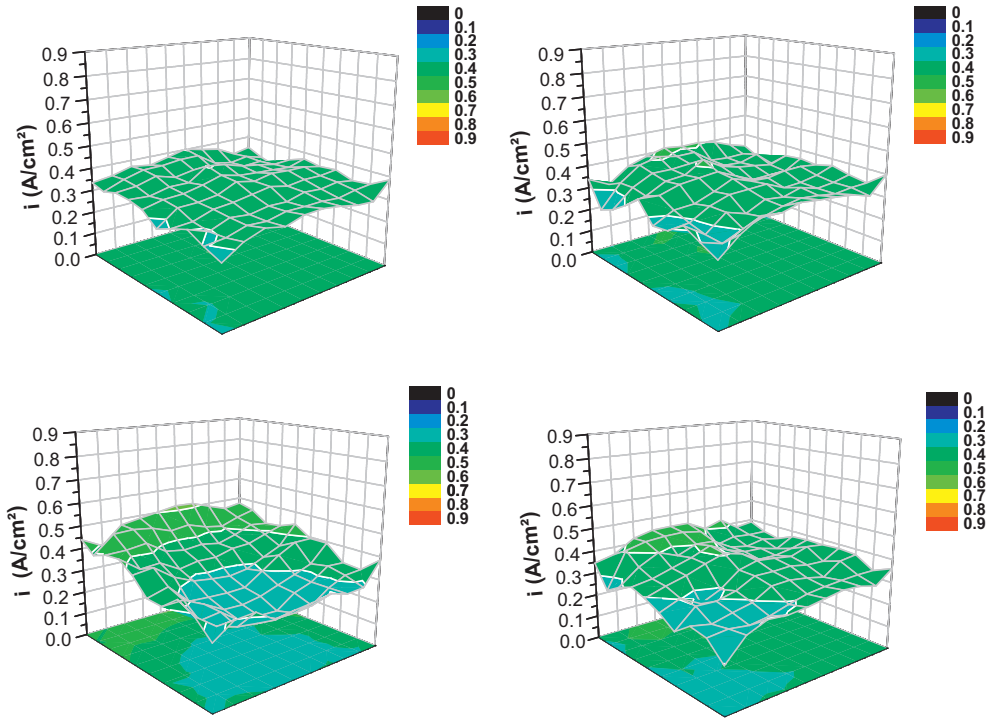

Fig. 12. Current distribution maps at an average current density of 0.325 A cm^{-2} under the flow conditions specified in Fig. 11. To find the correspondence between geometries and maps, refer to Fig. 4.

According to the data acquired, using deeper flow channels has no effect on fuel cell performance, while the wider channels lead to vaguely higher power at high current densities, probably for the simple reason that a bigger electrode area is covered by the channels this way. Current distribution maps were not conclusive as a very high spatial resolution is required to see such small differences.

4. Conclusions

The influence of flow channel geometry on the performance of a high temperature PEM fuel cell was analyzed. Four different configurations were investigated: 4 step serpentine, pin, parallel and interdigitated. Traditional polarization curves were accompanied by current distribution maps, which added very valuable information. Current distribution measurement was carried out using a sensor plate in a similar way that a segmented current collector. Neither electrodes nor flow field plates were segmented. Although the current density limits of the fuel cell could not be achieved due to equipment restrictions, the cell could be operated under mass transfer limitation conditions by regulating reactant flow rates. This way, the influence of flow channel geometry could be studied in the region where flow distribution is more important. Results show that, under the operational conditions employed in this work, a maximum power density up to 25% higher can be obtained if serpentine or pin-type flow channels are used when pure oxygen is the comburent. If the cathode is fed with air, the overall performance of the fuel cell gets worse due to the lower oxygen concentration. However, the new flux conditions make the interdigitated geometry remarkably improve its performance respecting the other configurations tested, reaching as good yields as serpentine or pin-type flow channels. Finally, it was observed that wider flow channels lead to slightly higher power when the system is working under high reactant demand conditions, while deeper channels have apparently no effect.

By means of the current distribution maps, it was possible to determine the weak points of a specific geometry or the reactant that is inducing mass transfer problems. This technique is then a good additional tool to progress in fuel cell design and to detect possible failures during operation.

Looking through different scientific works about flow channel geometry influence on conventional PEMFCs, it is found that the use of interdigitated flow channels lead to a superior performance due to the improvement in water removal from the porous media [26–28], which has also been predicted by means of modeling [29]. Serpentine flow channels are a good choice for water management, but yields are not as good as the achieved using the previous ones [15,26]. However pressure drop induced by flow channels and the facts that these statements cannot be applied to any operational conditions [30] have to be bore in mind before drawing any premature conclusion about which geometry is the most advisable. It seems to be clear that parallel flow channels should not be used under the operational conditions tested because of the existence of stagnant areas and bad use of electrode area, which is in consonance with results for the high temperature PEMFC. Regarding pin-type flow channels, preferential paths and inactive areas are expected if using them [14] and therefore lower performance is achieved experimentally [28]. Moreover, their low inherent pressure drop does not help water management so they can be discarded. Comparing this overview with the results obtained in this work for high temperature PEMFCs, one can find that the prospect is different. Interdigitated flow channels performance is comparable to serpentine only at high flow rates, probably because convective flux is not needed for water removal given the high temperature conditions. Furthermore, pin-type flow channels performance is as good as serpentine in every single experiment carried out. Current distribution maps obtained with this geometry are in some cases even more uniform than those get with serpentine flow channels, discarding dead electrode areas due to gas maldistribution. Therefore, according to this study, pin-type flow channels could be used when working at high temperature without expecting lower performance. In addition, pressure drop caused by pin-type flow channels is the lowest of the four geometries tested [25], which is important for its eventual real use in order to save on pumping costs.

Acknowledgements

The authors want to thank the Junta de Comunidades de Castilla-La Mancha (JCCM) for its financial support through the project PBI08-151-2045 and the Ministerio de Ciencia e Innovación (Ministry of Science and Innovation) for the grant AP2007-02713 awarded to Diego Úbeda as well as for the economical support received through the CICYT project CTM2007-60472.

References

[1] J.-H. Wee, Renew. Sust. Energy Rev. 11 (2007) 1720–1738.
[2] J. Hua, L. Xu, X. Lin, L. Lu, M. Ouyang, Tsinghua Sci. Technol. 14 (2009) 639–645.
[3] M. Saxe, A. Folkesson, P. Alvfors, Int. J. Hydrogen Energy 32 (2007) 4295–4305.
[4] M. Saxe, A. Folkesson, P. Alvfors, Energy 33 (2008) 689–711.
[5] J. Wu, X.Z. Yuan, H. Wang, M. Blanco, J.J. Martin, J. Zhang, Int. J. Hydrogen Energy 33 (2008) 1735–1746.
[6] J. Wu, X.Z. Yuan, H. Wang, M. Blanco, J.J. Martin, J. Zhang, Int. J. Hydrogen Energy 33 (2008) 1747–1757.
[7] K.-H. Hauer, R. Potthast, T. Wüster, D. Stolten, J. Power Sources 143 (2005) 67–74.
[8] D. Natarajan, T. Van Nguyen, AICHE J. 51 (2005) 2587–2598.
[9] A. Hakenjos, H. Muenter, U. Wittstadt, C. Hebling, J. Power Sources 131 (2004) 213–216.
[10] M. Noponen, T. Mennola, M. Mikkola, T. Hottinen, P. Lund, J. Power Sources 106 (2002) 304–312.
[11] T. Tingelöf, L. Hedström, N. Holmström, P. Alvfors, G. Lindbergh, Int. J. Hydrogen Energy 33 (2008) 2064–2072.
[12] S.J.C. Cleghorn, C.R. Derouin, M.S. Wilson, S. Gottesfeld, J. Appl. Electrochem. 28 (1997) 663–672.
[13] H. Sun, G. Zhang, L.-J. Guo, H. Liu, J. Power Sources 158 (2006) 326–332.
[14] X. Li, I. Sabir, Int. J. Hydrogen Energy 30 (2005) 359–371.
[15] W.-M. Yan, C.-H. Yang, C.-Y. Soong, F. Chen, S.-C. Mei, J. Power Sources 160 (2006) 284–292.
[16] J.-K. Kuo, T.-S. Yen, C.-K. Chen, Energy Convers. Manage. 49 (2008) 2776–2787.
[17] Ch. Wieser, A. Helmbold, E. Gülzow, J. Appl. Electrochem. 30 (2000) 803–807.
[18] M.V.S. Alvarez, Investigations of Current Density Inhomogeneities in Polymer Electrolyte Fuel Cells, ETH: Zurich, Swiss, 2006.
[19] M. Geske, M. Heuer, G. Heideck, Z.A. Styczynski, Energies 3 (2010) 770–783.
[20] D. Natarajan, T. Van Nguyen, J. Power Sources 135 (2004) 95–109.
[21] J. Lobato, P. Cañizares, M.A. Rodrigo, J.J. Linares, D. Úbeda, F.J. Pinar, Fuel Cells 10 (2010) 312–319.
[22] J. Lobato, P. Cañizares, M.A. Rodrigo, J.J. Linares, F.J. Pinar, Int. J. Hydrogen Energy 35 (2010) 1347–1355.
[23] J. Lobato, P. Cañizares, M.A. Rodrigo, J.J. Linares, G. Manjavacas, J. Membr. Sci. 280 (2006) 351–362.
[24] J. Lobato, P. Cañizares, M.A. Rodrigo, J.J. Linares, J.A. Aguilar, J. Membr. Sci. 306 (2007) 47–55.
[25] J. Lobato, P. Cañizares, M.A. Rodrigo, F.J. Pinar, E. Mena, D. Úbeda, Int. J. Hydrogen Energy 35 (2010) 5510–5520.
[26] T.V. Nguyen, J. Electrochem. Soc. 143 (1996) L103–L105.
[27] A. de Souza, E.R. González, J. Solid State Electrochem. 7 (2003) 651–657.
[28] S.-S. Hsieh, S.-H. Yang, J.-K. Kuo, C.-F. Huang, H.-H. Tsai, Energy Convers. Manage. 47 (2006) 1868–1878.
[29] X.-D. Wang, Y.-Y. Duan, W.-M. Yan, X.-F. Peng, Electrochim. Acta 53 (2008) 5334–5343.
[30] P.J. Hamilton, B.G. Pollet, Fuel Cells 10 (2010) 489–509.